PAPER • OPEN ACCESS

Dynamic and thermodynamic modulations of the convectively coupled equatorial waves by the MJO

To cite this article: Yan Zhu and Tim Li 2021 *Environ. Res. Commun.* **3** 025004

Environmental Research Communications

PAPER

Dynamic and thermodynamic modulations of the convectively coupled equatorial waves by the MJO

Yan Zhu[1,2] and Tim Li[1,2,*]

[1] Key Laboratory of Meteorological Disaster, Ministry of Education (KLME)/Joint International Research Laboratory of Climate and Environmental Change (ILCEC)/Collaborative Innovation Center on Forecast and Evaluation of Meteorological Disasters (CIC-FEMD), Nanjing University of Information Science and Technology, Nanjing, People's Republic of China

[2] Department of Atmospheric Sciences, and School of Ocean and Earth Science and Technology, University of Hawaii, Honolulu, Hawaii, United States of America

[*] Author to whom any correspondence should be addressed.

E-mail: timli@hawaii.edu

OPEN ACCESS

RECEIVED
27 October 2020

REVISED
24 February 2021

ACCEPTED FOR PUBLICATION
1 March 2021

PUBLISHED
17 March 2021

Keywords: Madden Julian oscillation, convectively coupled equatorial waves, tropical variability

Abstract

The convectively coupled equatorial waves (CCEWs), including the Kelvin, mixed-Rossby gravity (MRG), eastward inertio-gravity (EIG), and westward inertio-gravity (WIG) waves, are dominant synoptic-scale waves in the tropics. In this study, the modulation of the CCEWs by the MJO is examined with observational data from 1985–2005 over the Indian Ocean (IO), Maritime Continent (MC), and Western Pacific (WP). We find that the MRG wave is strengthened (weakened) to the west (east) of the MJO convection. In contrast, the Kelvin, WIG and EIG waves are mostly strengthened over the MJO convective center. As MJO modulates the background vertical wind shear and moisture fields, a further analysis was conducted to reveal the relationship between the background dynamic and thermodynamic field changes and the wave intensity change. A significant negative correlation between the MJO-scale vertical wind shear and the MRG intensity variation suggests that the MRG wave is primarily modulated by the dynamic field. The intensity changes of the WIG and EIG waves are significantly correlated to the MJO moisture field. The Kelvin wave, which has both quasi-geostrophic and gravity wave nature, is modulated by both the MJO-scale vertical wind shear and specific humidity.

1. Introduction

Convectively coupled equatorial waves (CCEWs) are characterized by the organized eastward or westward propagating cloud systems and significantly contribute to the synoptic-scale variability in the tropics. During their propagation, the CCEWs play an important role in tropical cyclone genesis (Bessafi and Wheeler 2006, Schreck *et al* 2011, Schreck *et al* 2012, Wu and Takahashi 2018), interaction with the MJO (Wang and Li 2017, Kikuchi *et al* 2018, Takasuka *et al* 2019), and modulation of diurnal rainfall variability (Baranowski *et al* 2016, Van Der Linden *et al* 2016, Chen *et al* 2019). Because of the vital influence of CCEWs on tropical weather and climate systems, enormous effort has been devoted to exploring the horizontal and vertical structure, propagation and evolution characteristics of the CCEWs (Yang *et al* 2003, Yang *et al* 2007a, 2007b, 2007c, Kiladis *et al* 2009, Yasunaga and Mapes 2012, Yuni *et al* 2019).

The Madden Julian Oscillation (MJO) is often described as a large-scale convective envelope with a planetary scale of circulation (Madden and Julian 1971, 1972, Li and Zhou 2009), a Kelvin and Rossby wave couplet structure (Hendon and Salby 1994, Adames and Wallace 2014), a vertically westward tilting structure (Sperber 2003, Hsu and Li 2012) and slow eastward propagating speed of 5–10 m s^{-1} (Wang 1988, Rui and Wang 1990). It is the dominant intraseasonal oscillation in the tropics. Nakazawa (1988) showed the hierarchical structure of the MJO convective envelope. Within the MJO convective envelope, there are eastward propagating super cloud clusters, which is comprised of the westward propagating individual cloud clusters. The hierarchical structure of the MJO envelope suggests that there is a strong coupling between the MJO and the CCEWs.

Although previous observational analyses revealed the fundamental features of the CCEWs and MJO, how they interact with each other is still an open question. Previous studies showed that the intensity of CCEWs depends on the MJO phase (Aiyyer and Molinari 2003, Roundy 2008, Yasunaga 2011, Dias *et al* 2013, Zhu *et al* 2019). Because of the large-scale nature of the MJO, the MJO can be regarded as a background state that affects the CCEWs. Previous works suggested that the MJO-scale zonal wind is a primary factor that affects the CCEWs (Zhang and Webster 1989, Wang and Xie 1996, Dias and Kiladis 2014). For example, in a two-level theoretical model, Wang and Xie (1996) showed that the vertical shear of zonal wind plays an important role in modulating the equatorial Rossby waves. Han and Khouider (2010) investigated the instability of the convectively coupled waves in a sheared environment with a simple multicloud model and noticed that different vertical shear profiles could destabilize different equatorial waves. The MJO-scale thermodynamic variable, such as specific humidity, is also regarded as an important factor in changing the characteristics of CCEWs (Lin *et al* 2008, Wang and Chen 2016, 2017). Wang and Li (2017) discovered that the phase speed of the convectively coupled Kelvin wave was greatly modulated by boundary layer moisture. However, most of these works were based on theoretical or intermediate models. In this study, we will investigate the relationship between CCEWs and MJO using an in-depth observational analysis. In particular, we will examine the scatter relationship between the intensity of the CCEWs and MJO-scale dynamic and thermodynamic fields separately. Through this analysis, we intend to reveal the roles of the dynamic and thermodynamic fields in modulating the intensity of different CCEWs.

The rest of the paper is organized as follows. The observational datasets and analysis methods used in this work are given in section 2. Section 3 shows the observed relationship between MJO and various CCEWs and possible mechanisms behind the observational phenomena. Finally, a conclusion and discussion are presented in section 4.

2. Data and methods

2.1. Data

The 20-year brightness temperature data from the Cloud Archive User Service (CLAUS) project (Hodges *et al* 2000) is used to conduct the frequency-wavenumber analysis similar as described by Wheeler and Kiladis (1999). The original data is three-hourly in time and 0.5° in horizontal resolution. In this analysis, we use the data spatially regridded into coarser resolution (1° latitude $\times$ 1° longitude) on the latitudinal bands between 20 °N–20 °S. The brightness temperature data is twice daily (0 h and 12 h), with period from 1985 through 2005. The interpolated outgoing longwave radiation (OLR) from the National Oceanic and Atmospheric Administration (NOAA) polar-orbiting satellites (Liebmann and Smith 1996) is used to describe the convective activity of the MJO. The atmospheric three-dimensional reanalysis data employed in this study are provided by European Centre for Medium-Range Weather Forecasts (ECMWF) reanalysis (ERA-Interim) (Dee *et al* 2011), including the zonal and meridional wind (u and v), vertical pressure velocity (ω) and specific humidity (q). The NOAA OLR and ECMWF reanalysis used in this study are daily data in the winter (November-April) of 1985–2005 with 2.5° $\times$ 2.5° spatial resolution.

2.2. Methods

A 20–100 day Lanczos band-pass filtering is utilized to extract the MJO signal (Duchon 1979). To achieve statistically significant results, MJO convective phases in three major activity regions are examined: tropical Indian Ocean (IO, 0°–10 °S, 85°–95 °E); Maritime Continent (MC, 5 °S–15 °S, 125°–135 °E); and tropical Western Pacific (WP, 5 °S–15 °S, 165°–175 °E) (figure 1(a)). An MJO active (suppressed) phase is defined when the box averaged OLR anomaly is smaller (larger) than one negative (positive) standard deviation (Hsu and Li 2012, Wang *et al* 2019). All of the diagnosis results are composed based on the difference between the MJO active and suppressed phase.

The CCEWs are extracted according to the spectral peaks in the wavenumber-frequency analysis of the brightness temperature data (Wheeler and Kiladis 1999) (figures 1(b), (c)). The wavenumber-frequency analysis is also conducted with the daily OLR data, which shows well analogous spectral peaks as those analyzed with brightness temperature data (figure not shown). Because there is an overlap of the frequency between the MJO and the Rossby wave, the Rossby wave is not investigated in this study. The specific CCEWs studied in this work are all on the synoptic time scale. They include the mixed-Rossby gravity (MRG), n = 0 eastward inertio-gravity (EIG), n = 1 westward inertio-gravity (WIG), and Kelvin waves. These CCEWs are extracted using the space-time filtering of a specific field. The field must represent the most essential feature of the CCEWs and is different for different waves. It is meridional wind for MRG wave, zonal wind for Kelvin wave and vertical velocity for n = 0 EIG and n = 1 WIG waves.

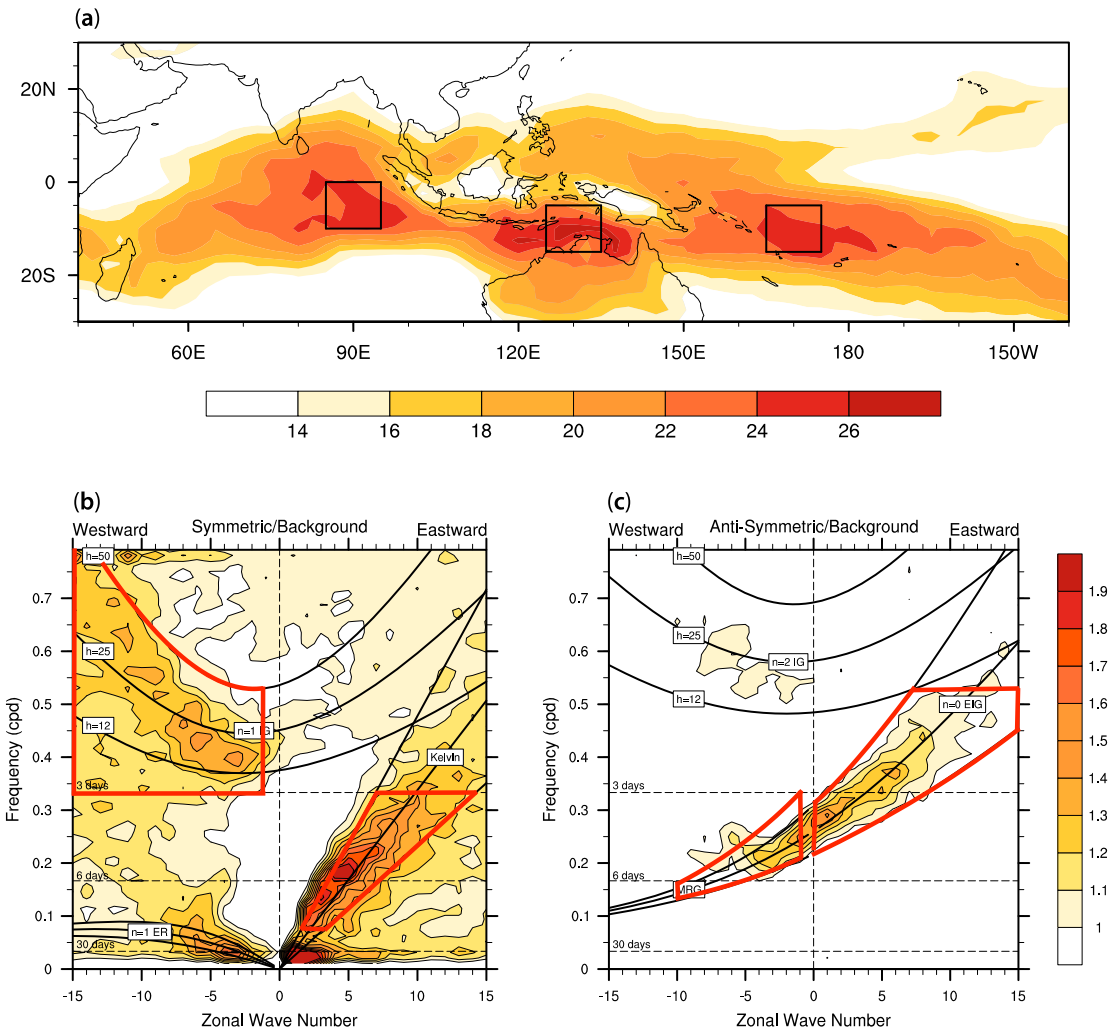

Figure 1. (a) The standard deviation of the 20–100-day filtered OLR (unit: W m^{-2}). The three black boxes indicate the regions to choose the MJO events: IO (0°–10 °S, 85°–95 °E), MC (5 °S–15 °S, 125°–135 °E) and WP (5 °S–15 °S, 165°–175 °E). (b) The wavenumber-frequency power spectrum of the symmetric component of brightness temperature between 15 °S–15 °N for January 1985 to December 2005, plotted as the ratio between raw brightness temperature power and the power in a smoothed red noise background spectrum. (c) as for (b), but for anti-symmetric component. The polygons indicated by the thick red lines are the wave-filtering bands for filtered waves. The band for the Kelvin wave is periods of 3 – 15 day, wavenumbers of 2 –14; The band for the n = 1 WIG wave is periods of 1 – 3 day, wavenumbers of −1 – −15; The band for the n = MRG is periods of 3 – 10 day, wavenumbers of −1 – −10. The band for the n = 0 EIG wave is periods of 2 – 5 day, wavenumbers of 0 – 15.

3. Modulation of the CCEWs by the MJO

The horizontal structures of the MJO convection and circulation in the three locations are presented in figure 2. The longitudes of the MJO convective centers are in 90 °E, 130 °E and 170 °E. In the IO, the MJO low-level flow reverses its direction at the MJO convective center, with westerly to the west and easterly to the east of the convective center. Zhang (2005) described this relationship between the MJO convective center and zonal wind as the MJO model I phase. When MJO moves to the MC and WP, the low-level westerly prevails over and to the west of the MJO convective center and a low-level easterly exists to the east of the convective center, which is similar to the MJO model II structure described in figure 6 of Zhang (2005). The vertical wind shear of the MJO circulation shows a dipole structure, and its phase coincides with the low-level flow, with easterly (westerly) shear occurring in the region of low-level westerly (easterly). The vertically integrated moisture anomaly field shows an in-phase spatial relation with the MJO convective center.

In order to test whether the chose specific fields can represent the different CCEWs, we use these fields as reference variables to regress the structures of the CCEWs. The 850 hPa space-time filtered specific field of each wave averaged over 5 °S–5 °N, 85°–95 °E is regressed against the 850 hPa winds and the OLR fields to obtain the composite structure of the waves (figures not shown). The regressed patterns of CCEWs in the IO are compared with their structures shown in Kiladis *et al* (2009). In Kiladis *et al* (2009), the structures of 850 hPa winds and the OLR are obtained by regressing onto the intraseasonal filtered brightness temperature in the Central Pacific.

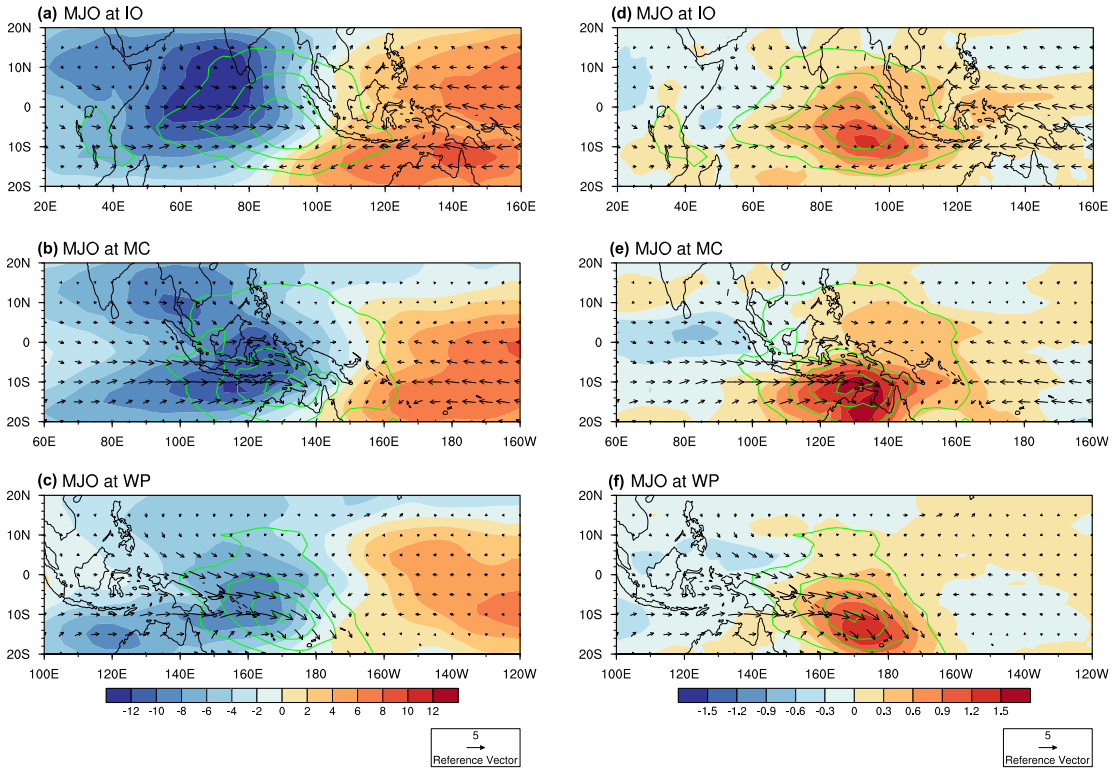

Figure 2. (a) Horizontal structures of MJO-scale vertical wind shear (shading, 200 hPa minus 850 hPa, unit: m s^{-1}), OLR (contour, unit: W m^{-2}) and 850 hPa wind anomalies (vector, unit: ms^{-1}) in IO (MJO active phase minus MJO suppressed phase). (b), (c) As in (a), but for the MC and WP regions. (d) Horizontal structures of vertically integrated (1000–300 hPa) MJO-scale specific humidity (shading, unit: g kg^{-1}), OLR (contour, unit: W m^{-2}) and 850 hPa wind anomalies (vector, unit: m s^{-1}) in IO (MJO active phase minus MJO suppressed phase). (e), (f) As in (d), but for the MC and WP regions.

Although we conduct regression with different reference variables and in different locations, the structures of the CCEWs display analogous features as shown in Kiladis *et al* (2009), which provides the confidence to use these specific fields to further investigate the modulation of MJO on the CCEWs. The structures of CCEWs in MC and WP are similar to IO but the intensity is weaker in the MC and stronger in the WP (figures not shown).

The specific field of the MRG wave, meridional wind, has a maximum value at the equator (Matsuno 1966, Chen and Huang 2009), so it is used as a proxy to measure how strong the MRG wave is modulated by the MJO. The difference in standard deviation (STD) of the MRG wave meridional wind between the MJO active and suppressed phase is presented to show such modulation. Because of the convective center of the MJO biases to the Southern Hemisphere in boreal winter, the center of the MRG wave's intensity change also appears more southward rather than in the equator. The STD difference of the MRG wave is averaged meridionally in the Southern Hemisphere where has maximum intensity change. The meridionally averaged STD differences of the MRG wave over the IO, MC and WP show a positive amplitude in the middle to lower troposphere with a maximum around 600 hPa (figure not shown). Figure 3(a) illustrates the horizontal pattern of the STD difference of the MRG wave at 600 hPa. The enhanced MRG wave activity appears to the west of the MJO convective center, and the weakened MRG wave intensity appears to the east.

The vertical velocity is chosen as the characteristic variable for $n = 0$ EIG and $n = 1$ WIG because vigorous upward motion is closely related to the convection of the IG waves. Unlike the MRG wave, the most pronounced variances of the IG waves manifest in the upper troposphere (figure not shown). Figures 3(b) and (c) show the STD differences of the vertical velocity field of the $n = 0$ EIG and $n = 1$ WIG waves between the MJO active and suppressed phase at 300 hPa. Although the convective center of the WIG wave locates over the equator and the convective centers of the EIG wave straddle the equator, both of their variance centers appear in the South Hemisphere because of the location of the MJO convective center. Unlike the MRG wave that has a dipole pattern (figure 3(a)), the maximum intensity change of the two IG waves concentrates over the MJO convective center.

Because the Kelvin wave has a maximum zonal wind at the equator, the zonal wind is selected as the characteristic variable to represent its intensity change. The vertical-longitude cross-sections of the STD difference of the Kelvin wave zonal wind indicate that the MJO modulation to the Kelvin wave is strongest near 600 hPa (figures not shown). Figure 3(d) shows the horizontal structure of the Kelvin wave modulated by the

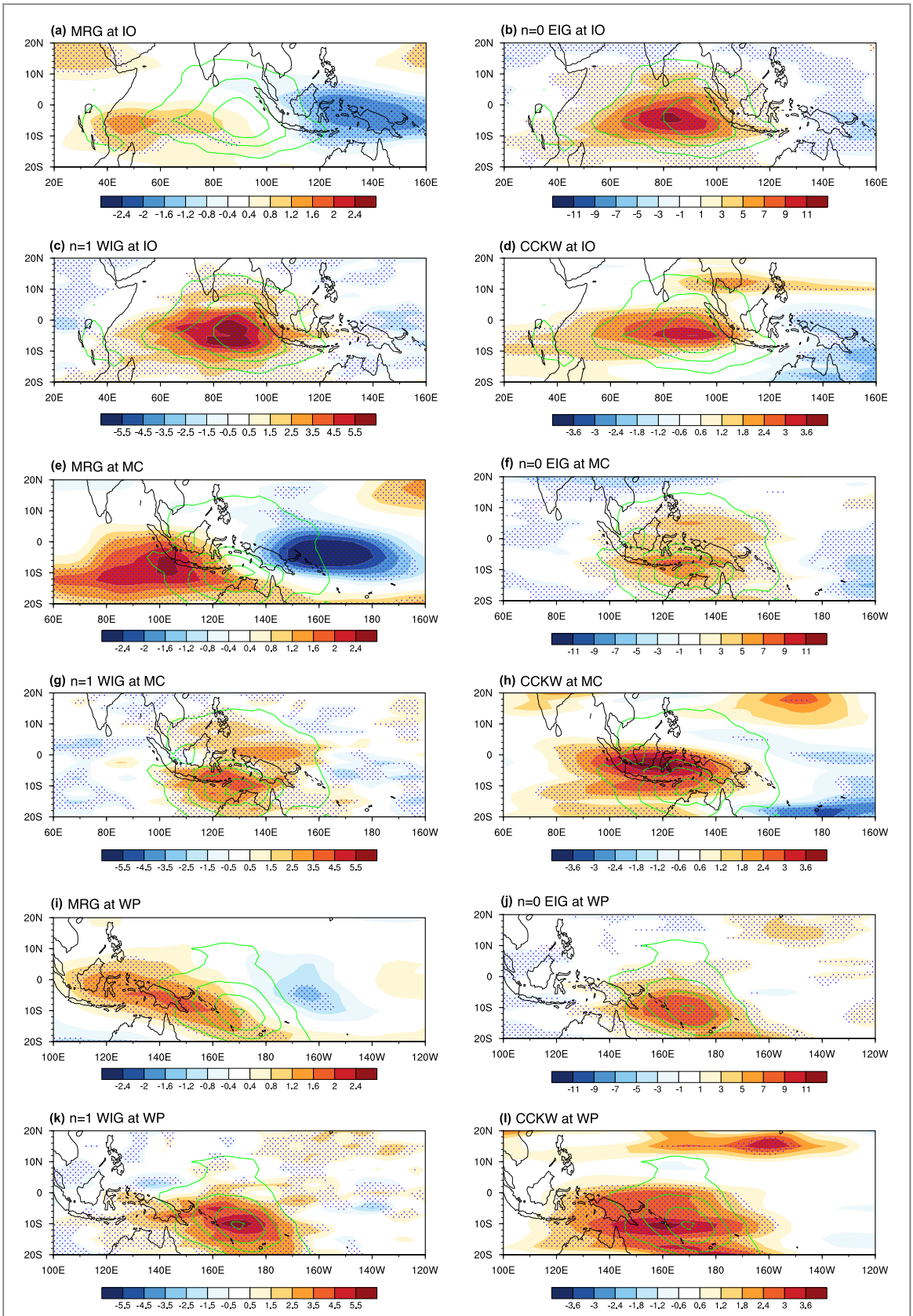

Figure 3. (a) Difference of standard deviation of MRG meridional wind at 600 hPa (shading, unit: 10^{-1} m s^{-1}) between MJO active and suppressed phase and the horizontal structure of the OLR anomalies (contour, unit: W m^{-2}) in the IO (MJO active phase minus MJO suppressed phase). (b), (c) As in (a), but for the n = 0 EIG and n = 1WIG waves vertical velocity (unit: 10^{-3} Pa s^{-1}) at 300 hPa. (d) As in (a), but for the Kelvin wave zonal wind at 600 hPa (shading, unit: 10^{-1} m s^{-1}). (e)–(h), (i)–(l) As in (a)–(d), but for the MC and WP regions.

MJO at 600 hPa. It exhibits a combined feature of MRG and IG waves. While a maximum wave intensity change appears over the MJO convective center, there is a clear east-west opposite change, with a weakened (strengthened) activity to the east (west) of the MJO convective center.

Compared to the IO, the intensity modulations of the four equatorial waves in the MC and WP display similar vertical and horizontal patterns. The maximum intensity changes in these two regions are located slightly southward owing to the fact that MJO centers shift further into the Southern Hemisphere (figures 3(e)–(h), (i)–(l)). Comparing with the other two regions, the intensity changes of the MRG and CCKW waves are relatively stronger and the intensity changes of the two IG waves are relatively weaker in the MC.

The different CCEWs show distinctive longitudinal distributions of intensity change which implies different MJO impacts on these waves. To determine to what extent the amplitude of an equatorial wave is controlled by the dynamic or thermodynamic field of the MJO, we plot a scatter diagram between the wave intensity change index and the MJO dynamic or thermodynamic field. We then focus on two MJO fields, vertical wind shear and specific humidity. Each of the three regions (60°–120 °E for the IO, 100°–160 °E for the MC, and 140 °E–160 °W for the WP) along the latitude of 0°–20 °S is divided into equally distributed boxes (10° in longitude). We also conducted the sensitivity tests with changes in the size of the boxes and found the size change did not affect the main result. The STD differences averaged in these boxes are defined as the wave intensity indices.

Figure 4(a) shows a scatter diagram of the intensity index for the MRG wave and MJO vertical wind shear averaged at each box. Different colors denote the three different regions (IO, MC and WP). To remove the MJO moisture effect, a partial correlation calculation is performed. It is noted that the intensity of the MRG wave is significantly correlated with the MJO vertical wind shear, with a high negative partial correlation coefficient (−0.83). However, no significant correlation is discovered between the intensity of the MRG wave and the MJO specific humidity (figure 4(b)). The result is congruous with the theoretical analysis of Wang and Xie (1996), who found that the background easterly (westerly) wind shear favors (inhibits) the development of the MRG wave in the lower troposphere through the coupling of the barotropic and baroclinic components of the MRG wave. However, the MRG wave is not sensitive to the change in background moisture because its wind field is large in the rotational component but weak in the divergent component.

Figures 4(c)–(f) indicate that the intensity changes of both the $n = 0$ EIG and $n = 1$ WIG waves have significant positive correlations with the MJO specific humidity, but not with the MJO vertical wind shear. The high correlations (about 0.85) between MJO specific humidity and the intensity of n=0 EIG and n=1 WIG waves can be explained by their dominant convergent component of the flows. There is higher background specific humidity field associated with an active phase of MJO so the two IG waves can converge more low-level moisture, which causes more condensational heating release and strengthens the wave intensity.

The relation between the Kelvin wave and the MJO background state is more complicated because the Kelvin wave has a semi-quasi geostrophic feature and a gravity wave nature. As a result, the Kelvin wave exhibits a significant correlation with both MJO vertical wind shear and specific humidity (figures 4(g)–(h)). Therefore, the Kelvin wave can be regarded as a special wave controlled by both the rotational and divergent flows. The enhanced (weakened) Kelvin wave activity to the west (east) of the MJO convective center seems not discussed in previous theoretical and modeling studies.

4. Conclusion and discussion

Tropical convection frequently occurs in different temporal and spatial scales, ranging from the diurnal cycle and CCEWs to MJO and ENSO. These multi-scale convective systems interact with each other. In this study, we investigate the modulation of the CCEWs by the large-scale MJO fields with observational data during 1985–2005. We focus on MJO activity over three key regions (IO: 0°–10 °S, 85°–95 °E; MC: 5°–15 °S, 125°–135 °E; WP: 5°–15 °S, 165°–175 °E), and examine the overall impact of the MJO on the CCEWs in these regions. A space-time spectral analysis of the brightness temperature is conducted, and different specific fields are used to extract four types of high-frequency CCEWs: MRG; $n = 0$ EIG; $n = 1$ WIG; and Kelvin waves.

Regardless of the MJO location (IO, MC or WP), the MRG wave is always enhanced (weakened) to the west (east) of the MJO convective center, where the MJO-scale easterly (westerly) shear dominates. On the other hand, the two IG waves are strengthened over the MJO convective center. The modulation of the Kelvin wave shows the feature combined with the MRG and IG waves. The Kelvin wave intensity is strengthened over and to the west but weakened to the east of the MJO convection.

The relative roles of the MJO dynamic and thermodynamic fields in modulating the equatorial waves are investigated through a scatter diagram analysis. The intensity of the MRG wave displays a statistically significant correlation with the MJO vertical wind shear but an insignificant correlation with the MJO specific humidity. The modulation of the MRG wave is in great contrast to the IG waves, which are significantly correlated with the MJO specific humidity but not significantly correlated with MJO vertical wind shear field. The MRG wave is

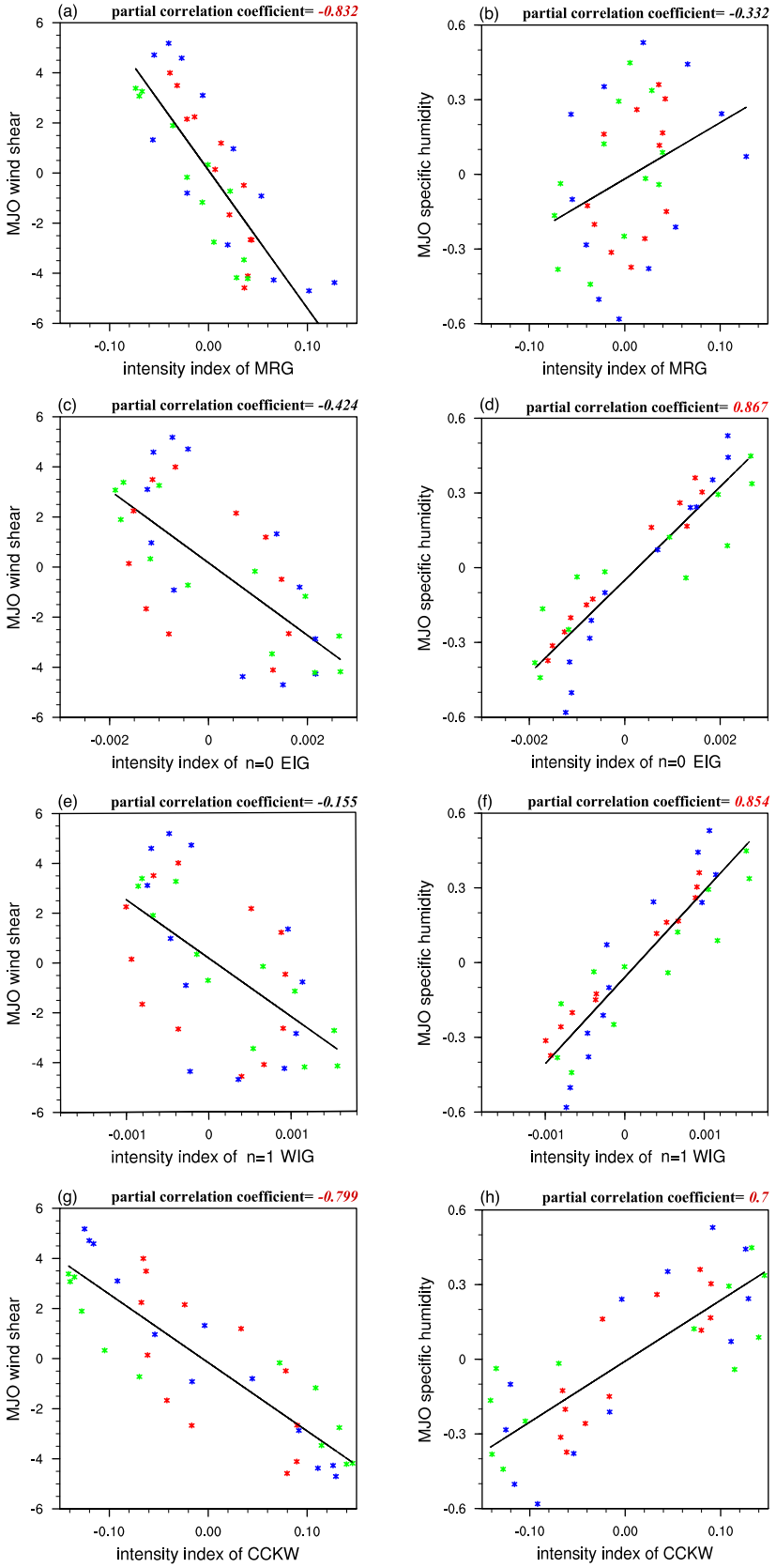

Figure 4. (a), (b) Scatter diagrams between the intensity index of the MRG and MJO vertical wind shear (left) and specific humidity (right). A partial correlation coefficient is shown in the top right of each panel. (c)–(h) As in (a), (b), except for the n = 0 EIG, n = 1 WIG and Kelvin waves. Red, blue and green asterisks indicate the values from IO, MC and WP, respectively. The black line represents the least squared regression fit.

dominated by rotational flow so that it is more sensitive to the forcing of vertical wind shear, whereas the IG waves are dominated by divergent flow so that they are more sensitive to diabatic heating induced by moisture convergence. Due to the coexisting natures of semi-quasi geostrophy and gravity wave, the Kelvin wave is sensitive to both the MJO dynamic (vertical wind shear) and thermodynamic (moisture) fields.

Previous studies showed that the current state-of-art climate models still have difficulty in simulating the observed CCEWs (Hung *et al* 2013, Wang and Li 2017), and there is a close relationship between the simulated MJO and the CCEWs (Guo *et al* 2015, Zhu and Li 2019). This study reveals the observed relationship between the intensity of the CCEWs and MJO vertical wind shear and specific humidity. Such observations may provide insight into how to improve the simulation of CCEWs intensity in the climate models.

Acknowledgments

This work was supported by NSFC grants (42088101, 41875069), NOAA grant NA18OAR4310298, and NSF AGS-1643297. This is SOEST contribution number 11289 and IPRC contribution number 1507.

Data availability statement

The data that support the findings of this study are available upon reasonable request from the authors.

ORCID iDs

Yan Zhu https://orcid.org/0000-0002-9198-4310

References

Aiyyer A R and Molinari J 2003 Evolution of mixed Rossby–gravity waves in idealized MJO environments *J. Atmos. Sci.* **60** 2837–55
Adames Ángel F. and Wallace John M. 2014 Three-Dimensional Structure and Evolution of the MJO and Its Relation to the Mean Flow *Journal of the Atmospheric Sciences* **71** 2007–26
Baranowski D B, Flatau M K, Flatau P J and Matthews A J 2016 Phase locking between atmospheric convectively coupled equatorial Kelvin waves and the diurnal cycle of precipitation over the Maritime Continent *Geophys. Res. Lett.* **43** 8269–76
Bessafi M and Wheeler M C 2006 Modulation of south Indian Ocean tropical cyclones by the Madden–Julian oscillation and convectively coupled equatorial waves *Mon. Weather Rev.* **134** 638–56
Chen G and Huang R 2009 Interannual variations in mixed Rossby–gravity waves and their impacts on tropical cyclogenesis over the western North Pacific *J. Clim.* **22** 535–49
Chen W-T, Hsu S-P, Tsai Y-H and Sui C-H 2019 The influences of convectively coupled kelvin waves on multiscale rainfall variability over the South China Sea and Maritime Continent in December 2016 *J. Clim.* **32** 6977–93
Dee D P *et al* 2011 The ERA-interim reanalysis: configuration and performance of the data assimilation system *Q. J. R. Meteorolog. Soc.* **137** 553–97
Dias J and Kiladis G N 2014 Influence of the basic state zonal flow on convectively coupled equatorial waves *Geophys. Res. Lett.* **41** 6904–13
Dias J, Leroux S, Tulich S and Kiladis G 2013 How systematic is organized tropical convection within the MJO? *Geophys. Res. Lett.* **40** 1420–5
Duchon C E 1979 Lanczos filtering in one and two dimensions *J. Appl. Meteorol.* **18** 1016–22
Guo Yanjuan, Waliser Duane E. and Jiang Xianan 2015 A Systematic Relationship between the Representations of Convectively Coupled Equatorial Wave Activity and the Madden–Julian Oscillation in Climate Model Simulations *Journal of Climate* **28** 1881–904
Han Y and Khouider B 2010 Convectively coupled waves in a sheared environment *J. Atmos. Sci.* **67** 2913–42
Hendon H H and Salby M L 1994 The life cycle of the Madden–Julian oscillation *J. Atmos. Sci.* **51** 2225–37
Hodges K, Chappell D, Robinson G and Yang G 2000 An improved algorithm for generating global window brightness temperatures from multiple satellite infrared imagery *J. Atmos. Oceanic Technol.* **17** 1296–312
Hsu P-C and Li T 2012 Role of the boundary layer moisture asymmetry in causing the eastward propagation of the Madden–Julian oscillation *J. Clim.* **25** 4914–31
Hung M-P, Lin J-L, Wang W, Kim D, Shinoda T and Weaver S J 2013 MJO and convectively coupled equatorial waves simulated by CMIP5 climate models *J. Clim.* **26** 6185–214
Kikuchi K, Kiladis G N, Dias J and Nasuno T 2018 Convectively coupled equatorial waves within the MJO during CINDY/DYNAMO: slow Kelvin waves as building blocks *Clim. Dyn.* **50** 4211–30
Kiladis G N, Wheeler M C, Haertel P T, Straub K H and Roundy P E 2009 Convectively coupled equatorial waves *Rev. Geophys.* **47** RG2003
Li T and Zhou C 2009 Planetary scale selection of the Madden–Julian oscillation *J. Atmos. Sci.* **66** 2429–43
Liebmann B and Smith C A 1996 Description of a complete (interpolated) outgoing longwave radiation dataset *Bull. Am. Meteorol. Soc.* **77** 1275–7
Lin J-L, Lee M-I, Kim D, Kang I-S and Frierson D M 2008 The impacts of convective parameterization and moisture triggering on AGCM-simulated convectively coupled equatorial waves *J. Clim.* **21** 883–909
Madden R A and Julian P R 1971 Detection of a 40–50 day oscillation in the zonal wind in the tropical Pacific *J. Atmos. Sci.* **28** 702–8
Madden R A and Julian P R 1972 Description of global-scale circulation cells in the tropics with a 40–50 day period *J. Atmos. Sci.* **29** 1109–23
Matsuno T 1966 Quasi-geostrophic motions in the equatorial area *Journal of the Meteorological Society of Japan. Ser. II* **44** 25–43
Nakazawa T 1988 Tropical super clusters within intraseasonal variations over the western Pacific *Journal of the Meteorological Society of Japan. Ser. II* **66** 823–39
Roundy P E 2008 Analysis of convectively coupled Kelvin waves in the Indian Ocean MJO *J. Atmos. Sci.* **65** 1342–59

Rui H and Wang B 1990 Development characteristics and dynamic structure of tropical intraseasonal convection anomalies *Journal of the Atmospheric Sciences* **47** 357–79
Schreck C J III, Molinari J and Aiyyer A 2012 A global view of equatorial waves and tropical cyclogenesis *Mon. Weather Rev.* **140** 774–88
Schreck C J III, Molinari J and Mohr K I 2011 Attributing tropical cyclogenesis to equatorial waves in the western North Pacific *J. Atmos. Sci.* **68** 195–209
Sperber Kenneth R. 2003 Propagation and the Vertical Structure of the Madden–Julian Oscillation *Monthly Weather Review* **131** 3018–37
Takasuka D, Satoh M and Yokoi S 2019 Observational evidence of mixed Rossby-gravity waves as a driving force for the MJO convective initiation and propagation *Geophys. Res. Lett.* **46** 5546–55
Van Der Linden R, Fink A H, Pinto J G, Phan-Van T and Kiladis G N 2016 Modulation of daily rainfall in southern Vietnam by the Madden–Julian oscillation and convectively coupled equatorial waves *J. Clim.* **29** 5801–20
Wang B 1988 Dynamics of tropical low-frequency waves: an analysis of the moist Kelvin wave *J. Atmos. Sci.* **45** 2051–65
Wang B, Chen G and Liu F 2019 Diversity of the Madden-Julian oscillation *Sci. Adv.* **5** eaax0220
Wang B and Xie X 1996 Low-frequency equatorial waves in vertically sheared zonal flow. Part I: stable waves *J. Atmos. Sci.* **53** 449–67
Wang L and Chen L 2016 Interannual variation of convectively-coupled equatorial waves and their association with environmental factors *Dyn. Atmos. Oceans* **76** 116–26
Wang L and Chen L 2017 Effect of basic state on seasonal variation of convectively coupled Rossby wave *Dyn. Atmos. Oceans* **77** 54–63
Wang L and Li T 2017 Roles of convective heating and boundary-layer moisture asymmetry in slowing down the convectively coupled Kelvin waves *Clim. Dyn.* **48** 2453–69
Wang L and Li T 2017 Convectively coupled Kelvin waves in CMIP5 coupled climate models *Clim. Dyn.* **48** 767–81
Wheeler M and Kiladis G N 1999 Convectively coupled equatorial waves: analysis of clouds and temperature in the wavenumber–frequency domain *J. Atmos. Sci.* **56** 374–99
Wu L and Takahashi M 2018 Contributions of tropical waves to tropical cyclone genesis over the western North Pacific *Clim. Dyn.* **50** 4635–49
Yang G-Y, Hoskins B and Slingo J 2003 Convectively coupled equatorial waves: a new methodology for identifying wave structures in observational data *J. Atmos. Sci.* **60** 1637–54
Yang G-Y, Hoskins B and Slingo J 2007a Convectively coupled equatorial waves. Part II: propagation characteristics *J. Atmos. Sci.* **64** 3424–37
Yang G-Y, Hoskins B and Slingo J 2007b Convectively coupled equatorial waves. Part I: horizontal and vertical structures *J. Atmos. Sci.* **64** 3406–23
Yang G-Y, Hoskins B and Slingo J 2007c Convectively coupled equatorial waves. Part III: synthesis structures and their forcing and evolution *J. Atmos. Sci.* **64** 3438–51
Yasunaga K 2011 Seasonality and regionality of the Madden-Julian oscillation and convectively coupled equatorial waves *SOLA* **7** 153–6
Yasunaga K and Mapes B 2012 Differences between more divergent and more rotational types of convectively coupled equatorial waves. Part I: space–time spectral analyses *J. Atmos. Sci.* **69** 3–16
Yuni A R E, Lubis S W and Setiawan S 2019 Vertical structure of convectively coupled equatorial waves (CCEWs) during Boreal summer and winter *IOP Conf. Series: Earth and Environmental Science (Bristol)* (IOP Publishing) 012010
Zhang C 2005 Madden-julian oscillation *Rev. Geophys.* **43** RG2003
Zhang C and Webster P J 1989 Effects of zonal flows on equatorially trapped waves *J. Atmos. Sci.* **46** 3632–52
Zhu Y and Li T 2019 Two-way interactions between MJO and high-frequency waves over the Maritime Continent in MJOTF/GASS models *Clim. Dyn.* **54** 1217–31
Zhu Y, Li T, Zhao M and Nasuno T 2019 Interaction between the MJO and high-frequency waves over the Maritime Continent in boreal winter *J. Clim.* **32** 3819–35